JACS
JOURNAL OF THE AMERICAN CHEMICAL SOCIETY
Article
pubs.acs.org/JACS

All-Atom Semiclassical Dynamics Study of Quantum Coherence in Photosynthetic Fenna–Matthews–Olson Complex

Hyun Woo Kim,[†] Aaron Kelly,[†,‡] Jae Woo Park, and Young Min Rhee*

Institute of Theoretical and Computational Chemistry, Department of Chemistry, Pohang University of Science and Technology, Pohang 790-784, Korea

Supporting Information

ABSTRACT: Although photosynthetic pigment–protein complexes are in noisy environments, recent experimental and theoretical results indicate that their excitation energy transfer (EET) can exhibit coherent characteristics for over hundreds of femtoseconds. Despite the almost universal observations of the coherence to some degree, questions still remain regarding the detailed role of the protein and the extent of high-temperature coherence. Here we adopt a theoretical method that incorporates an all-atom description of the photosynthetic complex within a semiclassical framework in order to study EET in the Fenna–Matthews–Olson complex. We observe that the vibrational modes of the chromophore tend to diminish the coherence at the ensemble level, yet much longer-lived coherences may be observed at the single-complex level. We also observe that coherent oscillations in the site populations also commence within tens of femtoseconds even when the system is initially prepared in a non-oscillatory stationary state. We show that the protein acts to maintain the electronic couplings among the system of embedded chromophores. We also investigate the extent to which the protein's electrostatic modulation that disperses the chromophore electronic energies may affect the coherence lifetime. Further, we observe that even though mutation-induced disruptions in the protein structure may change the coupling pattern, a relatively strong level of coupling and associated coherence in the dynamics still remain. Finally, we demonstrate that thermal fluctuations in the chromophore couplings induce some redundancy in the coherent energy-transfer pathway. Our results indicate that a description of both chromophore coupling strengths and their fluctuations is crucial to better understand coherent EET processes in photosynthetic systems.

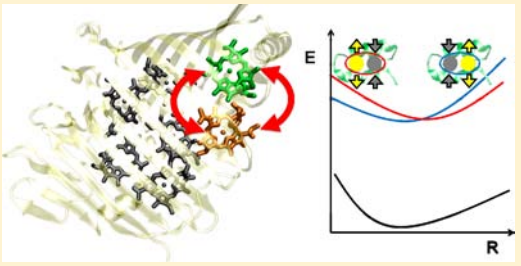

1. INTRODUCTION

Excitation energy transfer (EET) among chromophores is an important process during the early part of photosynthesis. Although it has been studied for many decades, many new results are still being discovered in both natural[1−5] and artificial[6−8] photosynthetic systems. Recently, it was revealed experimentally that EET in photosynthetic systems exhibits wave-like characteristic or quantum coherence for a few hundred femtoseconds.[1,2,9,10] Understanding this long-lived electronic coherence has subsequently become a paradigmatic subject in the photosynthesis research community.[11−13] Advances in experimental techniques, such as multidimensional electronic spectroscopy, have allowed observing quantum coherence in photosynthetic systems at cryogenic temperatures.[1,2] This was soon followed by additional observations of similar behaviors at physiological temperatures.[9,10] The research on quantum coherence has been frequently conducted with a relatively simple Fenna–Matthews–Olson (FMO) complex,[14] obtained from a light-harvesting green sulfur bacteria. The FMO complex, which controls the EET from outer antenna systems to the reaction center, consists of three monomer units with eight bacteriochlorophyll *a* (BChl) chromophores in each unit. Interestingly, FMO complex shows a reminiscent level of coherent oscillations at near-physiological temperature (277 K),[10] potentially leading to a debate on the general role of quantum coherence in photosynthetic systems. Moreover, how the protein facilitates the coherence is not well elucidated yet. In resolving such a debate and elucidating the protein's role, theoretical approaches shall prove useful as they are capable of providing microscopic views with potentially atomistic details. Indeed, numerous theoretical studies have been already reported and have provided useful insights on various aspects of the coherence.[15−25]

Theoretical approaches can be roughly classified in three different categories, as schematically illustrated in Figure 1. The first class ("Class I"; Figure 1a) is based on abstract models of the protein–chromophore complex.[16−23] In this type of approaches, chromophores are usually represented as excitable sites with a constant energy gap between the excited and non-excited states together with constant chromophore–chromophore couplings. The protein is simply represented as a heat bath, usually as a collection of harmonic oscillators. The chromophore–protein interaction is described in terms of predefined functional forms (typically bilinear in bath and

Received: March 29, 2012
Published: June 18, 2012

   dx.doi.org/10.1021/ja303025q | J. Am. Chem. Soc. 2012, 134, 11640−11651

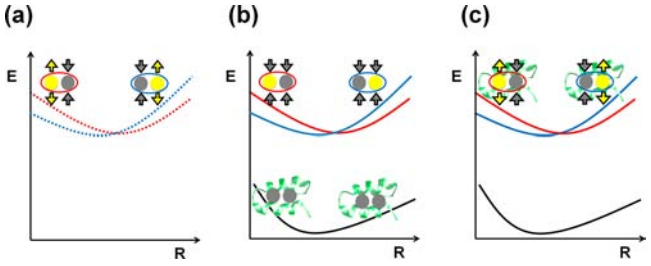

Figure 1. Schematic diagrams for explaining differences in three categories of theoretical approaches. The EET process within the single exciton manifold of a two-chromophore system is used for the illustration, with the chromophores represented with filled circles. **R** is the collective bath coordinate. Each curve represents a diabatic potential within site basis: a red (blue) curve corresponds to a state with the excitation on the left (right) chromophore. A black curve represents the ground-state manifold. Arrows represent the bath modes that surround the chromophores: yellow arrows represent the bath relaxed around an excited chromophore, while gray ones symbolize the bath relaxed around a non-excited chromophore. (a) A Class I approach is based on an abstract model of the bath, and the chromophore energies change by the coupling with the abstract bath. The bath modes are modeled differently for different states, and their relaxations can be correctly considered. (b) In a Class II approach, all-atom information (symbolically shown with a protein chain in green) is adopted, but the system Hamiltonian is obtained along ground-state trajectories. Thus, the bath modes always feel non-excited chromphores, and their relaxations with electronic transitions are not considered. (c) A Class III method is based on all-atom non-adiabatic trajectories and includes bath relaxation effects.

electronic coordinates) and generates the gap energy fluctuations. Due to their simplicity, the methods in this class are computationally efficient and, at the same time, can be numerically exact. Indeed, many important insights have been gained with such approaches: for example, noise-assisted energy transfer,[16] the possibility of quantum coherence at physiological temperature,[17] and long-lived quantum coherence at the single-complex level.[26] However, again due to the simplicity, they have inherent limitations in providing more fundamental views on the specific aspects of the photosynthetic EET process especially at the atomistic resolution. Very recently, there have been attempts to explicitly include the atomic protein degrees of freedom in the model,[24,25] which we categorize as the second class ("Class II"; Figure 1b). In Class II approaches, molecular dynamics (MD) simulations are performed in the ground state with all-atom information of pigment–protein complexes, followed by applications of semiempirical or quantum chemical methods to the snapshots along these MD trajectories for computing site energies. Using this information, non-adiabatic dynamics simulations are subsequently performed. Within the MD simulations, the all-atom information is incorporated using molecular force fields[27−29] majorly for computational efficiency. Olbrich et al. have applied this method to obtain conformational dependent site energies and couplings in the FMO complex and simulated its exciton dynamics and two-dimensional spectra.[24] Shim et al. have also studied exciton dynamics in FMO in a similar manner[25] and showed that the observed coherence was consistent with experimental[1,10] and simple model-based results.[17] At this level of description, the site energy fluctuations can be obtained in a more realistic manner than in the case of Class I approaches. However, Class II approaches cannot accurately describe bath relaxation dynamics associated with the exciton transfer process. Namely, because the protein only feels ground-state chromophores in the MD simulations, the site energy fluctuations and the related time-dependent Hamiltonian do not include the protein bath relaxation effect. In fact, including the bath relaxation is important[30,31] because it can affect the amount of coherence among chromophores.[32] To include the protein relaxation effect, the time evolution of the protein degrees of freedom should be obtained by considering different aspects of protein–chromophore interactions with different excitation states. Namely, the protein fluctuations need to be simulated simultaneously with the non-adiabatic EET dynamics. Such an approach constitutes the Class III method, as depicted in Figure 1c.

In this work, we have devised a Class III approach that includes the all-atom information and the protein relaxation during excited-state non-adiabatic simulations. For all-atom information, we adopted the conventional molecular force fields approach[27,28] similarly as in Class II methods. In our method, however, the protein bath relaxation is considered on a balanced footing with the exciton transfer dynamics through the Poisson bracket mapping equation (PBME).[33,34] Indeed, it has already been shown that PBME can describe the bath relaxation reasonably well,[34] and that it can be utilized to explain sub-picosecond coherent dynamics.[21] Through this semiclassical approach, we show that essential features of the coherence are also observed in the all-atom simulations. We also show that the somewhat exaggerated chromophore vibrations tend to diminish the coherence almost to an unnoticeable level. Nevertheless, the coherences with such vibrations in single FMO complexes endure rather long, implying that the room-temperature coherence may widely exist in nature without being noticed in ensemble measurements. In addition, we demonstrate that coherent and oscillatory EET still occurs even when the initial state is stationary. More importantly, by performing computational mutations to the proteins, we show that the major role played by the protein in the coherence is to maintain the structural regularity of the complex rather than to modulate the protein–chromophore electrostatic interactions. Even when the protein structure is partially distorted with mutations, the embedded chromophores still find strongly interacting conformations, leading to a modified but yet long-lived coherence. Implications of these findings are also discussed in regard to the biological role of coherence as concluding remarks.

2. MODELS

Since we are adopting an approach that is different from previously applied methods for studying the non-adiabatic EET process, it will be prudent to present the essence of our approach before discussing our findings. Here, we will briefly overview its basic features for treating the all-atom information in conjunction with the FMO model that we have adopted in this work. A more detailed technical description of the entire methodology is provided at the end of this article.

Model Hamiltonian. To account for the EET process with semiclassical non-adiabatic dynamics simulations, a Hamiltonian matrix with information of multiple excited states for the FMO complex is required. In this work, the Hamiltonian (H) has been constructed in the following way. (Its pictorial representation is also provided in Figure 2.) As we consider the EET process among seven BChls in an FMO monomer unit, the electronic subsystem is restricted to the subspace of single-excitations with a 7×7 dimensionality as in many other previous

dx.doi.org/10.1021/ja303025q | J. Am. Chem. Soc. 2012, 134, 11640−11651

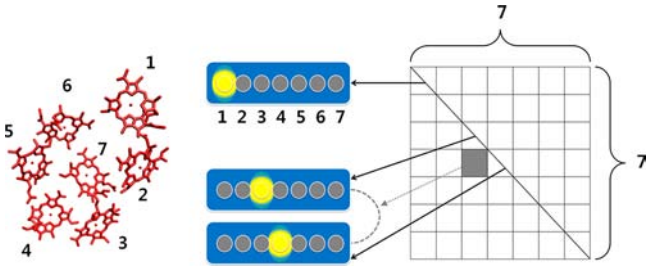

Figure 2. Pictorial illustration of the construction of the system Hamiltonian (H). Seven BChls in the FMO complex are drawn and numbered as 1−7 (left). For simplicity, the aliphatic tails of BChls are omitted. At right, gray and yellow circles represent BChls in the ground and excited states respectively, while the blue surrounding symbolically depicts the protein. A diagonal element, H_{11}, is calculated as the energy of the system when BChl-1 is excited with other BChls remaining in the ground state. An off-diagonal element, H_{43}, is the coupling between two states and is calculated from atomic distributions of transition dipoles of BChl-3 and BChl-4. All other matrix elements are calculated in similar manners.

studies.[17] The Hamiltonian matrix has atomic details with different expressions for the couplings and site energies for different conformations of the complex. For the off-diagonal coupling matrix elements, we adopt the transition-charge electrostatic potential (TrESP) method of Madjet et al.[35] This model distributes the molecular transition dipole to discrete atomic transition charges based on quantum chemical calculations, and has been shown[35] to be similarly accurate as continuous representation of the transition density[36] and as efficient as other approximate methods.[37] For this reason, TrESP has also been adopted in computing coupling strengths and their fluctuations in earlier studies.[24,37] For the diagonal matrix elements (site energies), we simply define them as the potential energies obtained with the conventional force field model[27,28] after properly exciting one of the seven chromophores.[35] For example, H_{11} is calculated as the energy of the system when BChl-1 is represented with the excited-state model while the other chromophores are represented with the ground-state model (see Figure 2). For this, force field models of BChl in two electronic states are needed.

The BChl atomic partial charges in the two states can be obtained by discretizing quantum chemically calculated electron distributions in the states. The discretization is a well-documented process (e.g., refs 38 and 39), and Madjet and co-workers have already reported such modeling based on density function theory (DFT) and time-dependent density functional theory (TDDFT) calculations.[35] To account for the effective screening effect by polarizabilities of protein−chromophore complex,[4,40,41] all partial charges and TrESP transition charges were scaled by a factor of 0.715. With this scaling factor, both the ground-state molecular dipole and the transition dipole become quite close to the experimentally measured values. We will use the dispersion parameters defined in the CHARMM27 set[27,28] for both ground and excited states of each BChl because dispersive nonbonded interaction is not as important as the electrostatic interaction for describing relaxation effect after electronic transition.[42−46]

With these electrostatic and dispersive models, BChl vibrational energy terms remain to be described. Low-frequency vibrations such as the butterfly motions of the porphyrin unit are in part already described properly by the intramolecular electrostatic interactions with the above-described state-dependent partial charges. Describing valence terms (bonding, bending, and torsion) is, however, somewhat tricky. The difficulty does not actually stem from the modeling as straightforward approaches are already known (e.g., ref 47). It is in fact related to the discrepancy between classical mechanics and quantum mechanics, and it becomes progressively more severe with increasing frequency. In classical mechanics, which we will adopt at least for obtaining configuration ensembles of the FMO complex, there is no vibrational zero-point energy. This deficiency leads to narrower distributions of displacements and momenta in high-frequency normal vibrational modes. Upon electronic transitions or the related EET, such a narrow distribution will introduce highly oscillatory behavior in the relaxation dynamics even with slight differences in the stable molecular geometries of the states before and after the electronic transition. Such fictitious oscillations occur as artifacts in high-frequency region, which have been observed in previous calculations of the spectral densities for the chromophores in the FMO complex[25,48] and with simulations of resolvation processes subsequent to chromophore excitation.[42] As a simple remedy, one may completely ignore the valence vibrations. Indeed, such an approach sometimes works better[42] and will likely work fine for small chromophores with small geometric differences in different electronic states. However, for large aromatic chromophores, this simple approach will omit certain low-frequency vibrational normal modes. For example, porphyrin ring breathing modes will have low enough frequencies that can be nearly properly described with classical mechanics. Considering these issues leads us to adopt two disparate approaches in a comparative manner: adopting (1) a model with the same valence vibrational descriptions for ground and excited states of BChl and (2) a model with different descriptions for the two states. The difference is incorporated by altering the equilibrium bond lengths of the excited BChl by changes from DFT to TDDFT optimized geometries. As alluded in the above, Model-1 will lead to an underestimation of the low-frequency vibrational effect, while Model-2 will likely induce an overestimation of the high-frequency effect with spurious appearances of high-frequency components. Shortly later, we will show that these indeed are the cases for the FMO complex in its various behaviors. Even though we cannot pinpoint the actuality due to the above-described limitations, we can still be assured that it lies within the range that we inspect. We will discuss various aspects of the coherent dynamics on this logical ground.

Model Validation. A potential concern that one may have with the above models is their degree of empiricism. However, it should be noted that much of the information is based on first-principle (TD)DFT calculations. In fact, similar approaches have been successfully applied to studying excited-state dynamics of biological systems such as DNA[49−51] and a luminescent chromophore−protein complex,[52] as well as resolvation dynamics associated with various chromophores.[42−46] To explicitly demonstrate the reliability of our models, let us present how they behave in reproducing a number of experimental and higher level computational features.

In Figure 3, the linear absorption spectrum is compared against experimental results.[53] Our spectrum was generated by taking the histogram of the energy eigenvalues of Hamiltonian matrices along 100 ns long ground-state MD trajectory of the FMO complex together with a constant shift for the peak center.[54] The figure shows that the linear absorption spectrum

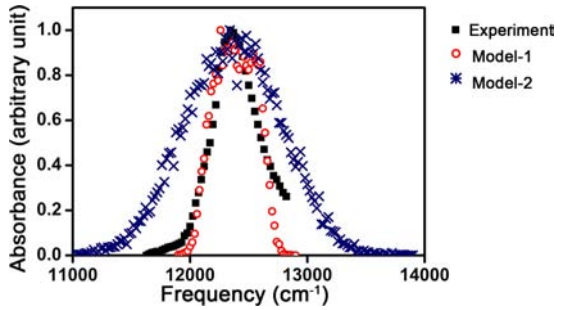

Figure 3. Comparison of experimental and simulated absorption spectra. For the simulated spectra, two different valence bond descriptions were adopted, as denoted as Model-1 and Model-2. The experimental absorption spectrum was taken from ref 53.

is indeed somewhat narrower with Model-1 and is wider with Model-2 when it is compared to the experimental peak. The widening is caused by the discrepancy between classical and quantal vibrations, and additionally by the lack of anharmonicity in Model-2.[42] In any case, it is encouraging that the experimental curve lies between the predictions from our two models, and that the Model-1 result matches it relatively well.

We have also compared the chromophore site energies from our models against previously reported values: quantum mechanical/molecular mechanical (QM/MM) calculation results reported by Shim et al.[25] and electrostatic modeling results by Adolphs and Renger.[15] In the more time-consuming but more reliable QM/MM approach, chromophores are free from empirical modeling beyond the approximate nature of the involved TDDFT calculations. In the electrostatic modeling case, the site energies have been obtained based on experimental optical spectra and thus closely reflect the experimental situation. By comparing site energies shown in panels a and b of Figure 4, one can see that our models are in decent to good agreements with the other approaches. Site 3 and site 6 energies are somewhat outlying compared to the experiment-based values. It is interesting to see that these two energies from our models are in close agreement with the QM/MM results. In fact, nearly all site energies from the QM/MM calculations are quite in good agreement with our results. Considering that our models and the QM/MM approach adopt different chromophore representations but the same type of protein representations, it is likely that the deviations from the experiment-based values are caused by the limitations in the protein representation. For example, the lack of polarizability in the protein model might have caused such discrepancies. In this work, instead of attempting to minimize the discrepancies with a much more computationally demanding protein representation such as the polarizable force field, we have taken a practical approach of estimating the extent to which the site energy deviations are affecting the coherent dynamics. For this purpose, we have additionally performed simulations by applying constant shifts to the site energies to eliminate all the deviations from the experiment-based values. As will be explained in the next section, we observe that this shifting has only marginal effect on the coherent dynamics. In any case, it is again encouraging that our simple models are well mimicking the site energies from the more sophisticated QM/MM (TDDFT) results.

When the site energy fluctuations are compared to the TDDFT case, Model-1 somewhat underestimates the fluctuations while Model-2 overestimates them, implying that the actual amount should be in between the values from our two models (Figure 4). In this case, it should be noted that the overestimation of the site energy fluctuation with Model-2 is

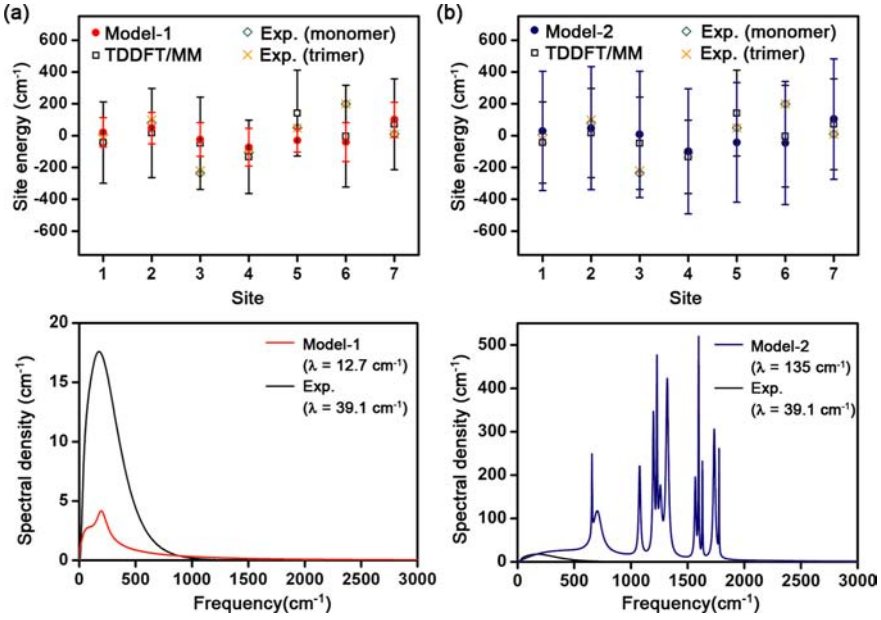

Figure 4. Site energy fluctuations and spectral densities obtained with (a) Model-1 and (b) Model-2. Site energies (top panels) are drawn so that the average value over all seven sites becomes identical throughout different models. In general, the average site energies from our models are very similar to the results from more demanding and yet more reliable TDDFT-based calculations, and our two models correctly constitute the upper and lower bounds of the TDDFT-based site energies. Site energies obtained from electrostatic modeling based on experimental optical spectra are also compared. The overall trend is in good agreement with two noticeable outlying sites. The spectral densities and the related reorganization energies from our two models also exhibit similar bounding behaviors (bottom panels). TDDFT results are adopted from ref 25, and the experimental site energies and spectral density are based on Adolphs and Renger's model in ref 15.

dx.doi.org/10.1021/ja303025q | J. Am. Chem. Soc. 2012, 134, 11640−11651

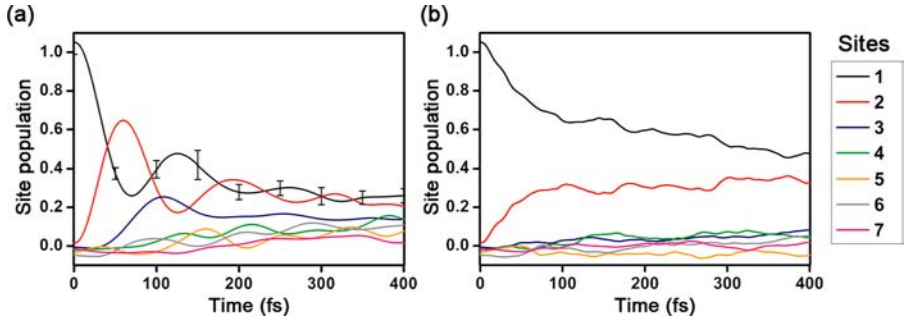

Figure 5. Population dynamics after exciting BChl-1 with the two valence vibration models. (a) When the chromophore vibration effect is silenced with Model-1 with the same valence bond potential of ground- and excited-state BChls, the population transfer pattern is quite coherent. (b) With Model-2 with different descriptions for excited and nonexcited BChl vibrations, the population dynamics is much less oscillatory. In (a), the error bars display the standard deviations ($\pm\sigma$) in the BChl-1 populations. Similar amounts of errors were observed in all other population dynamics throughout this work.

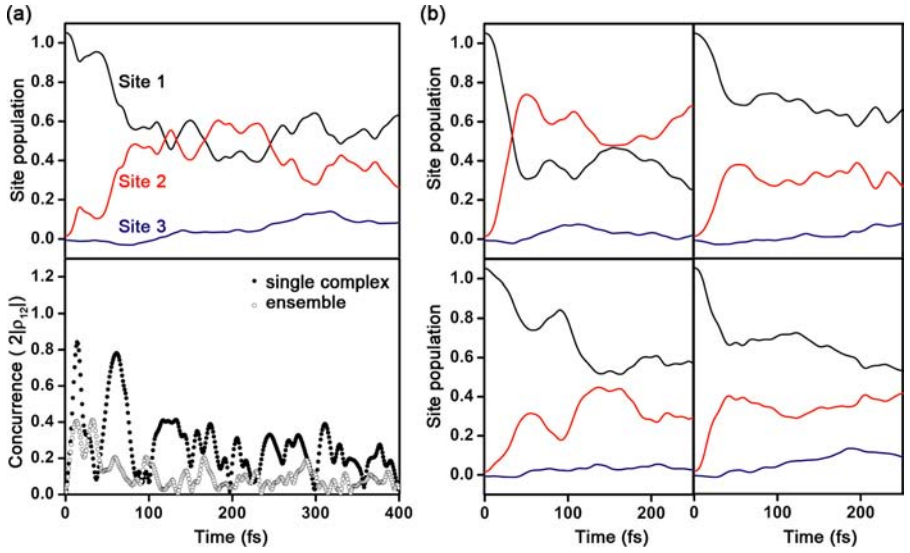

Figure 6. (a) Population dynamics and concurrence at the single-complex level simulated with Model-2. The population transfer pattern is quite oscillatory and the concurrence is much larger than in the ensemble case, showing that the single-complex coherence is more noticeable than in the ensemble. (b) Four other single complexes exhibit similar oscillatory behaviors with different oscillating patterns. Thus, we can see that coherence is lost majorly due to ensemble dephasing. For visual clarity, only populations of BChls-1−3 are shown.

mainly from the lack of anharmonicity of the chromophore valence vibrations. These site energy fluctuations can be further utilized for computing the spectral density which reflects the protein−chromophore coupling strength. In Figure 4, the spectral densities are compared against Adolphs and Renger's model based on experimental information. Again, one can see that the actuality lies in between our two models. With the vibrational effects, high-frequency component is in general exaggerated with strong spurious peaks as we expected in the above. The associated reorganization energies (λ) are 12.7 cm^{-1} with Model-1 and 135 cm^{-1} with Model-2. The experiment-based value lies in between, at λ = 39.1 cm^{-1}. Based on these observations, we can infer that our two models are indeed reasonable upper and lower bounds for describing realistic chromophore−protein interactions with atomic details.

3. RESULTS AND DISCUSSION

Coherence in FMO. We have first simulated the EET dynamics after initially exciting BChl-1 within the two limiting models as described in the previous section. In fact, the EET pathway after the initial excitation at BChl-1 is a well studied topic with the FMO complex.[15−25] Figure 5 shows that the population transfer patterns from Model-1 and Model-2 are noticeably different in the appearance. The population transfer profile is quite coherent (Figure 5a) with Model-1, where the same valence bond potentials are adopted for both ground- and excited-state BChls. The coherent beating in the population dynamics persists for ∼300 fs as was found in many simple model-based (Class I) simulations with the FMO system,[17,19−23] even though the populations in the long time limit are somewhat deviating due to the PBME limitation.[21] On the other hand, the population beating is observed only to a reminiscent level when ground and excited BChls were described with different valence vibrations (Figure 5b). This difference can be easily rationalized by considering the reorganization energies from the two models. With different vibrational potentials with Model-2, the reorganization energy is larger than with Model-1 as the chromophore vibrations can additionally modulate the site energy fluctuations. Of course, with a larger reorganization energy, the coherent oscillation in the population transfer becomes diminished[20,23,31,55] as is evidently shown in Figure 5. As explained in the previous section, the initial conformations for our PBME simulations were obtained with classical MD trajectories, and the

dx.doi.org/10.1021/ja303025q | J. Am. Chem. Soc. 2012, 134, 11640−11651

vibrational effect is somewhat exaggerated in Model-2. Accordingly, the reality with the FMO complex will lie in between the two cases. This aspect is in a sense in line with a recent experimental report with a marine algae system by Scholes and co-workers, which indicated that the vibrational coherence may exist in the population dynamics but seemingly to a lesser degree than the electronic contribution.[56]

As explained in the previous section, when constant shifts are added to the Hamiltonian to eliminate all the site energy deviations from the experiment-based values, the nature of coherence in the population dynamics are only marginally affected with similar oscillations on all populations. (See Figure S1 in Supporting Information.) Namely, the coherent beating persists for ∼300 fs or longer with Model-1, while it exists only to a reminiscent level with Model-2. Because the actuality will lie in between the two models, one may be concerned that the level of coherence in the FMO complex can be almost negligible in all-atom simulations if the actuality is quite close to the case of Model-2. However, one should notice that Figure 5 was obtained with an ensemble of 2000 independent PBME trajectories. Because there are quite many degrees of freedom in FMO, the population dynamics may have become less coherent due to different behaviors from different ensemble members. In fact, Ishizaki and Fleming have recently suggested (with a Class I approach) that the quantum coherence can remain much longer at the single-complex level.[26] With our all-atom model, we also observe long-lived coherence at the single-complex level even when the chromophore vibration is explicitly included with Model-2, by taking a single conformation of the complex and simulating 2000 independent PBME trajectories from it with as many different initial conditions for the quantum degrees of freedom. As is shown in Figure 6a, the oscillation in the population persists up to a few hundred femtoseconds when a single conformation of the complex is adopted in this manner. This long-lived coherence is additionally evidenced with the relatively large concurrence,[57] defined in terms of the off-diagonal elements of the density matrix[58] to represent the degree of coherence in the system. When the single-complex level simulations are continued on different conformations of FMO, we can observe similarly long-lasting coherences but with different oscillation patterns (Figure 6b). The concurrences also persist for well over 100 fs in all cases (Figure S2). Our results clearly demonstrate that the coherence is participating in the EET process over a long time period and that the individual photosynthetic complexes can be behaving even more coherently than is observed with ensemble measurements, where the dephasing effect washes out the individual oscillations. It should be stressed that we are presenting these single-complex coherences within the description based on Model-2, which acts as the lower bound for observing the coherence effect. Therefore, the actual single-complex coherence will likely be even more drastic than is shown in our simulations.

The Nature of the Initial Excitation. Even though we observed long-lived coherence at the single-complex level, one may wonder that it is an inherent result from the adopted initial condition as we have assumed that the excitation energy is localized at BChl-1 at time zero. In fact, this initial state is a superposition of eigenstates of the Hamiltonian which will definitely oscillate in time. Even in experiments, initial states have been prepared as coherent superposition states[1,9,10] with coherent light sources which may strongly affect the ensuing dynamics.[59]

Therefore, it will be instructive to examine the behavior of the system when it is initially generated in a non-oscillating stationary state. In all-atom simulations, this can be relatively easily achieved by using the eigenstate of the total Hamiltonian at any given conformation. Of course, when we tested such an initial condition with PBME by fictitiously fixing the Hamiltonian as constant, there were no oscillations in populations. When we have adopted the actual Hamiltonian with Model-1, the coupled BChls now display beating behaviors after 20−30 fs as shown in Figure 7. The oscillating pattern is

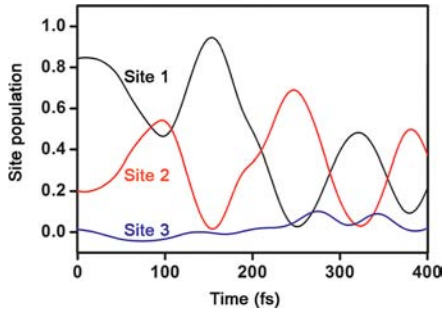

Figure 7. Population dynamics of an initially stationary exciton state at 300 K. Coherent beating is still found after ∼20 fs time delay.

also similar to the previously shown case with Figure 5a except the fact the oscillation persists much longer here as it is based on a single complex. This suggests that the time-dependent fluctuation of the Hamiltonian is fast enough to drive the initially stationary state into an oscillating superposition state. Here, the fluctuations in the Hamiltonian components will be the driving force toward inducing oscillations.[18] We also note that the adopted model (Model-1) in this case neglects portions of fluctuations from chromophore vibrational effects. In reality, when the missing portions actually participate in perturbing the Hamiltonian, the oscillation will likely commence even earlier.

Of course, showing that the coherence can generally exist regardless of the nature of the initial preparation would require much more extensive studies with inspections with widely varying initial conditions. At the very least, however, our results indicate that the fluctuations around the chromophores are much faster than the observed coherence time scale (a few hundred femtoseconds), and even a stationary state will be rendered into an oscillating state within a few tens of femtoseconds.

Protein's Role in Coherence. Up to this point, we have focused on the relationships of coherence with the choromophore vibration and with the initial condition. In a sense, similar aspects can also be investigated with simple model-based Class I approaches, and there have actually been many such reports on the coherent dynamics itself[16−23] and its enhancement at the single-complex level.[26,60] The real benefit of applying a much more demanding Class III approach as in our work will be the detailed information that can be obtained with the realistic representation of the protein−chromophore complex. From this part on, we will present a detailed look on the role of the protein and other aspects during the coherent EET process analyzed in atomic resolution. As discussed in a previous part, the chromophore vibration can significantly conceal the coherence when observed at the ensemble level. Therefore, in the following discussion with ensemble observations for protein characteristics, we will exclusively

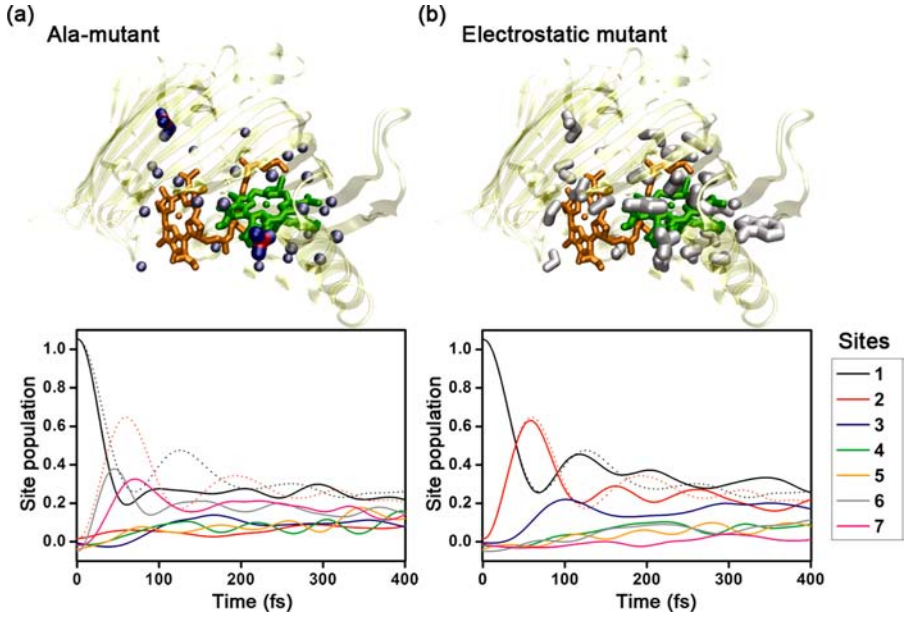

Figure 8. Schematic illustrations of two mutated FMO complex structures and their EET population dynamics: (a) Ala mutant and (b) electrostatic mutant. BChl-1 and BChl-2 are shown in green and orange, and side chains of the protein residues that are in contact with the two chromophores are overlaid explicitly. To facilitate a direct comparison, the population dynamics from the wild-type protein (shown in Figure 5a) is also presented with dotted lines.

adopt Model-1 with the same valence bond description for ground- and excited-state BChls.

For the purpose of understanding the protein's role, we have computationally mutated it in two manners. The first system, simply referred as the Ala mutant, was developed to consider the structural confinement effect on the chromophores from the protein. This mutant was generated by substituting with alanines (Ala) for 27 charge-neutral residues in close proximity to BChl-1 and BChl-2 as shown in Figure 8a. (See Computational Details for more information.) The second mutant was modeled to modulate the electrostatic interactions between BChls and the protein, and was generated by resetting the entire protein atomic partial charges to zero. In this way, all atoms in 359 residues of the protein which are listed in the crystal structure are affected (Figure 8b). When PBME simulations were performed, these two modified systems exhibited markedly different behaviors as shown in Figure 8. When the spatial confinement effect of the protein on BChl-1 and BChl-2 is altered, the coherent beating between these BChls is not observed. Instead, likely due to chromophore realignment, BChls-1, -6, and -7 display a coupled behavior. On the contrary, the electrostatic distortion does not significantly alter the EET profile when the excitation is initially localized on BChl-1.

This result may be surprising as it is well known that the transition energy fluctuations are caused primarily by electrostatic interactions between the environment and the dipole moment change of the chromophore. In fact, such aspect has been continuously observed with prototypical chromophores in polar solvents.[42−46,61,62] Similarly to polar solvents, the protein would also show a stochastically fluctuating charge distribution especially from alternating conformations and tune the site energies of the chromophores.[15] However, the overall protein electrostatic effect observed in our simulations was only marginal. This implies that the protein electrostatics is not the major source of site energy modulations for BChls which are importantly participating in the EET pathway initiated from BChl-1.

To consider the site energies of mutants in detail, we compared the site energies of the two mutants with the wild type (Figure 9). In Ala mutant, where the BChl-1 and BChl-2

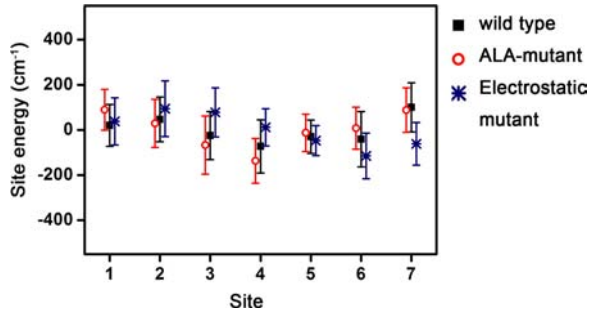

Figure 9. Site energies within the wild-type protein and the two adopted mutants. The average energy of all seven sites is set to be zero for each pigment−protein complex.

are not as tightly embedded as in the wild-type case, the site energies are only slightly affected. This is natural as the protein electrostatics is only slightly affected by this mutation. In contrast, the site energies in the electrostatic mutant are noticeably modified at BChl-3, -4, -6, and -7. With the initial excitation localized on BChl-1, the population transfer pattern is only slightly affected because the early coherent dynamics largely depend on the nature of BChl-1 and BChl-2 which are rather insensitive to the electrostatic mutation.

The sensitivity to the structural effect (Ala mutation) is not from the site energy modulation but from the coupling modulation. This can be clearly demonstrated when the coupling strengths among chromophore pairs are compared. In the wild-type FMO complex, the coupling between BChl-1 and BChl-2 varies around -110 cm^{-1} with a narrow width of σ = 15 cm^{-1} (Figure 10a). However, the same coupling fluctuates

dx.doi.org/10.1021/ja303025q | J. Am. Chem. Soc. 2012, 134, 11640−11651

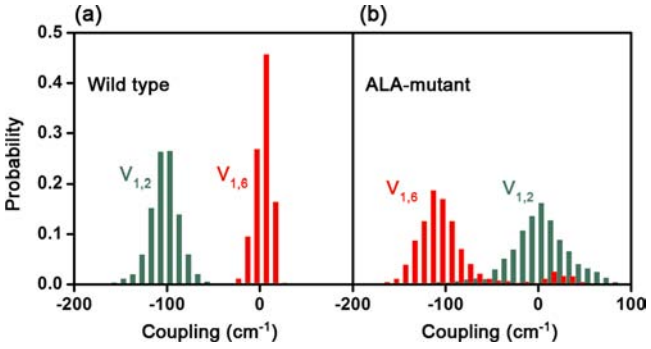

Figure 10. Distributions of BChl-1:BChl-2 coupling ($V_{1,2}$) and BChl-1:BChl-6 coupling ($V_{1,6}$) (a) in the wild-type protein and (b) in the Ala mutant.

more with the Ala mutant around 0 cm^{-1}. In addition, the BChl-1:BChl-6 pair, which exhibited coherent beating pattern in their population dynamics with the Ala mutant (Figure 8a), shows strong coupling with a large width in the mutant case (Figure 10b). This shows that the coherence is mainly affected by the coupling strength. Of course, the width or the fluctuation in the coupling will affect the detailed aspect of the coherence,[63] as will be discussed in a later part of this section. Thus, even without the spatial correlation of the atomic motions in the FMO complex,[64] coherence may still persist as long as there is strong enough coupling over the coherence time scale. In fact, any pair that is coupled at the initial excitation will remain coupled for hundreds of femtoseconds because any BChl coupling is mainly governed by their relative orientation and distance, which may not vary fast due to the protein scaffold.

The insensitivity of the coherent pattern within the electrostatic mutant does not necessarily mean that the population transfer will always be insensitive to the electrostatic modulation. As mentioned in the above, the energies of BChl-3, -4, -6, and -7 are strongly affected by the electrostatic mutation. Thus, the EET dynamics may be more severely altered when the excitation is localized on BChl-6 initially. In fact, such an aspect was already predicted by Müh et al.,[65] who reported that protein helices can modulate the EET pathway and that those helices are near BChls that are importantly participating for EET initiated from BChl-6.[65] When we performed PBME simulations with the initial excitation localized on BChl-6, indeed, we observed that the population pattern changed to a larger extent than in Figure 8b. (See Supporting Information and Figure S3 for details.) Interestingly, even in this case, the coherent aspect and the related oscillations are not seriously affected as there are still strongly coupled chromophore pairs.

In any case, it should be noted that the site energy fluctuations are not strongly affected by the electrostatic mutation. In Figure 9, the BChl site energies exhibit similar standard deviations (~100 cm^{-1}) in both the wild type and the electrostatic mutant. This similarity in the site energy fluctuation can be a result of the intramolecular electrostatic interaction within the choromophores. Upon electronic transition, the charge distribution within BChl evidently changes. Accordingly, for differently varying geometries of BChl, the energies of the ground and the excited states change in different ways. This induces gap energy fluctuations with continuous motions of the chromophores, and it is contributing to the major portions of the site energy fluctuations as shown in Figure 9. Moreover, at 300 K, it can be inferred from Figure 4 that the energy fluctuation in any one BChl is generally larger than the site energy differences among different BChls. These differences among the seven BChls (or the site energy "dispersion") mainly result from the protein electrostatic effect. Of course, the chromophore vibrations will get suppressed at low enough temperatures and the site energy dispersion will likely become more important than the fluctuation. Thus, in the low temperature limit, the site energy tuning from the protein may become a governing factor for enhancing EET.[15,66] However, at least in the 300 K case that we have tested, the site energy fluctuation is larger than the dispersion and its major portion is induced by the chromophore motions. These factors are actually causing the similar behaviors in population dynamics from the wild type and from the electrostatic mutant (Figure 8b).

In a sense, the Ala mutant that we have examined is a system with drastic changes. One might even question the biological relevance of testing such a severely "damaged" complex with 27 mutated residues. We have seen that the Ala mutant loses the native coherent coupling between BChl-1 and BChl-2 and instead gains the non-native one between BChl-1 and BChl-6. This fact suggests that the structural regularity gained by the protein scaffold is a key factor for preserving the energy-transfer pathway.[67] It additionally implies that the quantum coherence may still be observed even when the protein structure is partially damaged. It is very likely that there will be some pairs that are tightly and coherently coupled when BChls are well oriented with reasonable intermolecular distances as in FMO. In such a condition, structural distortion or damage may still result in an alternate coupling pattern as in the case of BChl-1 to BChl-6 coupling within the Ala mutant. In that sense, it is

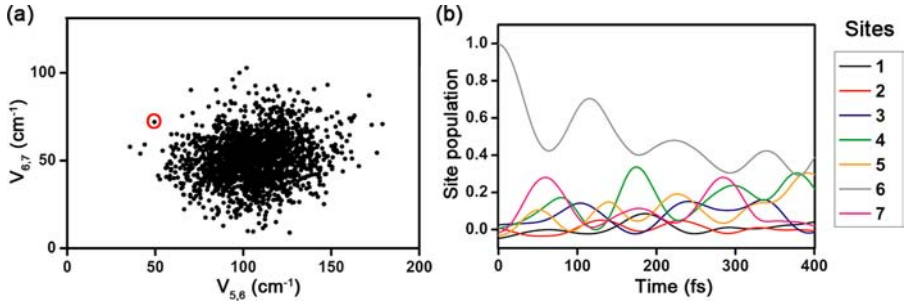

Figure 11. (a) Fluctuations of BChl-5:BChl-6 ($V_{5,6}$) and BChl-6:BChl-7 ($V_{6,7}$) couplings from an equilibrium ensemble of 2000 FMO conformations. (b) EET pattern initiated from a conformation with small $V_{5,6}$ and large $V_{6,7}$, marked with a red circle in (a). Overall, the energy flows in a sequence of BChls-6→7→4.

dx.doi.org/10.1021/ja303025q | J. Am. Chem. Soc. 2012, 134, 11640−11651

possible that this condition is related to fidelity in the energy transfer, and the quantum coherence will apparently be linked with such aspects.

Coupling Fluctuation and EET Pathway Redundancy. By analyzing the role of the protein, we have shown that the coupling strength is very important in governing the coherence. We have also shown that the coupling pattern may change drastically with modifications on the protein. However, even the wild-type protein without any mutation will have couplings with fluctuating characteristics at physiological temperature. As our approach can describe such variations straightforwardly, we can further investigate how the fluctuation in the coupling is affecting the EET process. For this purpose, we have inspected energy-transfer patterns after initially exciting BChl-6.[68] On average, BChl-6 exhibits significant couplings with BChl-5 and BChl-7.[15] The EET process from BChl-6 has also been frequently investigated both with experiments and theories.[17,21,25,67]

When the BChl-6:BChl-7 and BChl-6:BChl-5 couplings are inspected from an ensemble of 2000 conformations, both display quite a range of fluctuations (Figure 11a). In general, the trend is in agreement with the widely adopted model[16−22] with larger BChl-6:BChl-5 coupling and smaller BChl-6:BChl-7 coupling. However, because of the large range of fluctuations, sometimes BChl-6:BChl-7 coupling becomes significantly larger. When one such conformation was chosen and non-adiabatic PBME simulations were subsequently performed, not surprisingly, the energy flowed roughly through a sequence of BChls-6→7→4 (Figure 11b), instead of the more generally accepted 6→5→(7,4) path. Again, this aspect clearly shows that BChl-6 can transfer excitation energy to BChl-5 or BChl-7 depending on the coupling strength, and we can infer that there is some level of redundancy in the EET pathway. Of course, the redundancy will add a level of robustness to the biological function of the complex. We can also infer that consideration of the fluctuating aspect of the chromophore coupling will be important in gaining the complete picture of the energy-transfer process.

4. CONCLUSION

We have successfully performed semiclassical non-adiabatic simulations of a photosynthetic FMO complex with all-atom details, and investigated essential features of the coherent dynamics in the complex. By adopting two extreme ways of describing chromophore vibrations, we could establish upper and lower bound models that can correctly encompass the actual situation with the coherence. With the chromophore vibrations affecting the energy-transfer dynamics, we showed that a dephasing effect hampers the measurement of coherence at the ensemble level. However, the hidden coherence at the single-complex level persists for much longer time. With our approach with atomistic details, indeed, this dephasing effect could be demonstrated in a straightforward manner. Namely, population dynamics initiated from different conformations showed different energy-transfer patterns, and the oscillation in any single complex lasted longer than in the ensemble case. This suggests that the actual coherence may be longer lasting than was previously deduced with experiments especially at high-temperature conditions, where the environmental effect on dephasing will become severe.

The above simulations were carried out from initially coherent states, which will by design oscillate in time. Thus, we also inspected the behavior of an initially stationary excitonic state of a single FMO complex. Even with reduced fluctuating perturbations with silenced chromophore vibrations, coherent oscillations ensued within a few tens of femtoseconds. Because there are many different possibilities for initially exciting the pigment−protein complex, we admit that more in-depth studies will be needed to fully understand the impact of the initial state preparation on the accompanying quantum coherence. Of course, single-complex level investigations will be crucial for performing such studies and applying theoretical approaches like in our study will be fruitful. We also note that single-complex level experiments for complex but coherent systems are becoming feasible these days. For instance, Hildner et al. demonstrated with organic dyes that the quantum coherence could in fact be observed in single-molecule type experiments and suggested that similar approaches should also be applicable to photosynthetic pigment−protein complexes.[69]

To elucidate the role of the protein, we prepared two mutant systems which are deficient in either structural or electrostatic characteristics of the wild-type protein. Out of the two variations, removing the electrostatic interaction displayed a noticeable but not significant change in the coherence along the population dynamics. When the initial excitation was localized on a site whose energy was severely affected by the electrostatic modification, changes in the population dynamics were more pronounced. In contrast, structural disruption exhibited significantly altered coherences in the population transfer pattern. Interestingly, even when the protein structure was partially distorted, coherence was still observed because chromophores coupled in an alternative manner by reorienting themselves. Therefore, we can conclude that the steric effect of the protein scaffold maintains the chromophore configurations and plays a key role of keeping the coherence in the natively defined way over the sub-picosecond time scale. This steric nature preserves the coupling to a significant level even at high temperatures. In addition, from the altered coherence in the structurally disrupted mutant, we can infer that coherence may be robust against changes in the protein, as long as the change is not as severe as to block the assembly of the chromophores. This is because chromophores separated with reasonable spacings may find strongly coupled partners with a relative ease.

The chromophore coupling also exhibits noticeable fluctuations as a result of the thermal motion of the pigment−protein complex. These fluctuations may of course induce variations in population transfer patterns and will also be a source of dephasing effect in the ensemble. Occasionally, the fluctuation is large enough to alter the EET pathway as the ordering in coupling strengths is changed. Therefore, there is a certain level of redundancy in the EET pathway and this redundancy may possibly enhance the robustness of photosynthetic EET processes. Thus, we infer that both the strength and the fluctuation of chromophore couplings play important roles in photosynthetic systems by providing fidelity and robustness in the energy-transfer processes.

Like many theoretical approaches, our method has a number of intrinsic limitations. As we are adopting an approximate mixed quantum-classical approach, the resulting coherences do not fully reflect quantum mechanical phenomena. For example, it is well known that the PBME populations in the long time limit deviate from correct values.[21] Artifacts from classical vibrations are also related to this aspect. The polarizability of the protein and the chromophore is also an important feature that was only implicitly included in our models. As the polarization has a role of screening the electrostatic interactions

and the dipolar coupling between chromophores, it will likely affect the detailed coherent dynamics during the EET process. Overall, however, our approach provides a way of improving existing methods for considering the all-atom aspect of the dynamics at a much more reasonable cost than the computationally formidable full quantum mechanical treatments. Methods for more adequately considering vibrations and polarizations are continuously developed,[4,25,70,71] and we believe our approach can be further extended as a more accurate and more efficient tool for simulating coherence in biological systems, potentially with a capability of exhibiting reliable long time dynamics. This will surely help us to understand the biological meaning of the coherence during photosynthetic EET processes, and hopefully such biological meaning may find utility in designing artificial light harvesting systems in the future.

5. COMPUTATIONAL DETAILS

Semiclassical Dynamics. We are primarily interested in the dynamics of the quantum subsystem (the exciton) and the bath (all atoms in the system) which can be integrated simultaneously. To this end, we have employed Poisson bracket mapping equation (PBME),[33,34] which was explicitly formulated by Kapral and co-workers as a variant of mixed quantum-classical Liouville theory.[72] In this approach, the bath and the quantum subsystem degrees of freedom are propagated together according to forces acting on multiple excited states after mapping the quantum degrees of freedom to harmonic oscillators. (See Supporting Information for more details.) Briefly, PBME has the following nominal form,

$$\frac{\mathrm{d}}{\mathrm{d}t}B_{\mathrm{m}} = iL_{\mathrm{m}}^{0}B_{\mathrm{m}}$$

where B_{m} is a general observable in the mapping basis. The approximate Liouville operator, L_{m}^{0} is obtained from the full quantum-classical Liouville operator by omitting a term that is equal to one-quarter of the back reaction of the quantum subsystem on the bath.[34] This deficiency will not significantly affect our descriptions as we are focusing on the coherence effect in the short time regime in this study.

For initial conditions, we assume that the initial density may be decomposed into quantum subsystem and bath components ($\rho = \rho_{\mathrm{sys}}\rho_{\mathrm{bath}}$). The initial bath configurations can be obtained from various conformations in the ground-state MD simulations of the pigment–protein complex. This is a reasonable approach as the natural photosynthetic systems are in the ground state right before the start of the EET process. For the quantum subsystem, depending on the simulation conditions, the initial excitation is localized on one of the chromophoric sites or is dispersed over multiple chromophores as a nonoscillatory excitonic state.

With the all-atom Hamiltonian as described in a previous section (Figure 2), the semiclassical trajectories were calculated with the PBME formalism as further explained in ref 21 and the Supporting Information. We selected 2000 conformations along a trajectory of 100 ns ground-state MD simulation to obtain the initial conformations of 2000 independent PBME trajectories. With this ensemble size (2000), the statistical uncertainties in populations measured with 2σ were mostly under 0.10. While this level of error may lead to too large (>1.0) or too small (<0.0) populations, coherent dynamics tend to exhibit even larger oscillations as can be exemplified with Figure 5. Even though increasing the sampling size will of course eliminate such statistical errors, we have found that the computational cost and the accuracy are in balance with this sampling size. The time step for integrating PBME was 0.1 fs. In total, for the PBME dynamics, we have utilized ~50 years of aggregate CPU time at a supercomputer cluster with Intel Xeon X5570 processors. The computation was performed with an in-house built program supplemented by GROMACS[73] library for efficiently calculating molecular interactions.

Molecular Dynamics Simulations. The FMO complex from *Chlorobaclum tepidum* (PDB code: 3BSD)[74] was parametrized using the CHARMM27 force field with CMAP corrections[27,28] and with supplemental parameters for bacteriochlorophyll *a* (BChl) taken from the work of Foloppe et al.[75] The atomic partial charges and transition charges for the ground and excited states of BChls were derived from the DFT results of Madjet and co-workers.[35] With these parameters, we performed classical MD and semiclassical simulations. Since the eighth BChl does not associate well with the monomeric complex, as seen in previous MD studies of this system,[24] it was omitted in this study. In addition, the FMO complex with seven BChls has been frequently adopted as a representative system for theoretically studying quantum coherence.

In classical MD simulations, a monomeric pigment–protein complex with seven BChls was placed in a periodic cubic box with TIP3P water with 100 Å at each side. The system was initially equilibrated for 10 ns after energy minimization, followed by a production run for 100 ns with 2 fs time step. In this simulation, hydrogen atoms were constrained with the LINCS algorithm.[76] From this production run, 2000 frames were sampled at equal time spacing for the subsequent semiclassical simulations. Because we have adopted a flexible TIP3P water model in the semiclassical simulations, these 2000 conformations were further equilibrated with 0.5 ps MD simulations with 0.1 fs time step after replacing the rigid TIP3P with the flexible one. The force constants for the bond stretch and the angle bending of flexible TIP3P were 1200.80 kcal/mol·Å^2 and 150.10 kcal/mol·rad^2. All MD simulations were performed using GROMACS.[73] In these simulations, the temperature and the pressure of the system were held at 300 K and 1 atm by the weak coupling methods of Berendsen.[77] Long-range electrostatic interactions were described by the particle mesh Ewald (PME) method[78] using a cutoff distance of 12 Å. The cutoff distance for the van der Waals interaction was chosen to be 8 Å with smooth tapering to zero at 10 Å. Neighbor search was performed at every 10 steps with cutoff distance of 12 Å.

Preparation of Mutant Systems. The mutant systems that we adopted to reveal the role of protein were generated in the following manners. In considering the electrostatic modifications on the protein, we have taken a simple approach of setting the protein atomic partial charges to zero. The same initial conformations as the wild-type simulations were employed in the subsequent semiclassical simulations. To elucidate the spatial effect of the protein near the chromophores, a mutant of the FMO complex was prepared by changing neutral residues near BChl-1 and BChl-2 to alanines. This was performed by substituting all charge neutral residues within 4 Å from the two chromophores according to the crystal structure. A glycine residue (Gly219) was within this range but was excluded from the substitution. The void space generated by these substitutions was filled with water molecules. The same MD protocols as in the wild-type protein complex were adopted for generating initial conditions for semiclassical simulations with this mutant system.

Vibrational Effect and Spectral Density. In order to study the effect of the chromophore vibrations, we computed the equilibrium bond lengths of the ground and excited BChls with B3LYP[79,80] and time-dependent B3LYP together with the 6-31G(d,p) basis set. The quantum chemical calculations were performed with a developmental version of Q-Chem 4.0.[81] From these bond lengths, we set up two valence bond models as explained in a previous section. These models can also be adopted for calculating spectral densities, which can subsequently be used for estimating reorganization energies. Eleven additional MD trajectories of 100 ps durations were performed together with the same protocols with the bond-constraining simulations. The initial structures of these runs were chosen from the 100 ns production run at equal time spacing. Along each trajectory, conformations were saved every 2 fs and were later adopted in computing the time correlation function of BChl-1 site energy fluctuations. Following Olbrich et al.,[48] time correlation functions were fitted to an analytic functional form and corresponding spectral densities were calculated. (See Supporting Information for more details.) When obtaining the reorganization energy, we carried out a

numerical integration in the domain of frequency between 0 and 5000 cm^{-1}.

■ ASSOCIATED CONTENT

Supporting Information

Complete refs 27 and 81; details of PBME dynamics, population dynamics with shifted site energies, concurrences of single complexes, additional energy flow pattern in the electrostatic mutant, and fitted parameters for time correlation function of site energy fluctuations. This material is available free of charge via the Internet at http://pubs.acs.org.

■ AUTHOR INFORMATION

Corresponding Author

ymrhee@postech.ac.kr

Present Address

‡Department of Chemistry, Stanford University, Stanford, CA 94305

Author Contributions

†H.W.K. and A.K. contributed equally to this work.

Notes

The authors declare no competing financial interest.

■ ACKNOWLEDGMENTS

This work was supported by WCU Program (Grant No. R32-2008-000-10180-0) and Basic Science Research Program (Grant Nos. 2009-0067085 and 2011-0023393) through the National Research Foundation of Korea, funded by the Ministry of Education, Science, and Technology. The supercomputer time from Korea Institute of Science and Technology Information under Grant No. KSC-2011-C2-30 is also gratefully acknowledged. H.W.K. is a recipient of TJ Park Graduate Fellowship.

■ REFERENCES

(1) Engel, G. S.; Calhoun, T. R.; Read, E. L.; Ahn, T.-K.; Mančal, T.; Cheng, Y.-C.; Blankenship, R. E.; Fleming, G. R. *Nature* **2007**, *446*, 782−786.

(2) Lee, H.; Cheng, Y.-C.; Fleming, G. R. *Science* **2007**, *316*, 1462−1465.

(3) Adolphs, J.; Müh, F.; Madjet, M. E.-A.; Schmidt am Busch, M.; Renger, T. *J. Am. Chem. Soc.* **2010**, *132*, 3331−3343.

(4) Curutchet, C.; Kongsted, J.; Muñoz-Losa, A.; Hossein-Nejad, H.; Scholes, G. D.; Mennucci, B. *J. Am. Chem. Soc.* **2011**, *133*, 3078−3084.

(5) Strümpfer, J.; Şener, M.; Schulten, K. *J. Phys. Chem. Lett.* **2012**, *3*, 536−542.

(6) Utschig, L. M.; Silver, S. C.; Mulfort, K. L.; Tiede, D. M. *J. Am. Chem. Soc.* **2011**, *133*, 16334−16337.

(7) Terazono, Y.; Kodis, G.; Bhushan, K.; Zaks, J.; Madden, C.; Moore, A. L.; Moore, T. A.; Fleming, G. R.; Gust, D. *J. Am. Chem. Soc.* **2011**, *133*, 2916−2922.

(8) Castagna, R.; Garbugli, M.; Bianco, A.; Perissinotto, S.; Pariani, G.; Bertarelli, C.; Lanzani, G. *J. Phys. Chem. Lett.* **2012**, *3*, 51−57.

(9) Collini, E.; Wong, C. Y.; Wilk, K. E.; Curmi, P. M. G.; Brumer, P.; Scholes, G. D. *Nature* **2010**, *463*, 644−647.

(10) Panitchayangkoon, G.; Hayes, D.; Fransted, K. A.; Caram, J. R.; Harel, E.; Wen, J.; Blankenship, R. E.; Engel, G. S. *Proc. Natl. Acad. Sci. U.S.A.* **2010**, *107*, 12766−12770.

(11) Ishizaki, A.; Calhoun, T. R.; Schlau-Cohen, G. S.; Fleming, G. R. *Phys. Chem. Chem. Phys.* **2010**, *12*, 7319−7337.

(12) Scholes, G. D. *J. Phys. Chem. Lett.* **2010**, *1*, 2−8.

(13) Scholes, G. D.; Fleming, G. R.; Olaya-Castro, A.; van Grondelle, R. *Nature Chem.* **2011**, *3*, 763−774.

(14) Fenna, R. E.; Matthews, B. W. *Nature* **1975**, *258*, 573−577.

(15) Adolphs, J.; Renger, T. *Biophys. J.* **2006**, *91*, 2778−2797.

(16) Mohseni, M.; Rebentrost, P.; Lloyd, S.; Aspuru-Guzik, A. *J. Chem. Phys.* **2008**, *129*, 174106.

(17) Ishizaki, A.; Fleming, G. R. *Proc. Natl. Acad. Sci. U.S.A.* **2009**, *106*, 17255−17260.

(18) Rebentrost, P.; Mohseni, M.; Kassal, I.; Lloyd, S.; Aspuru-Guzik, A. *New J. Phys.* **2009**, *11*, 033003.

(19) Huo, P.; Coker, D. F. *J. Chem. Phys.* **2010**, *133*, 184108.

(20) Tao, G.; Miller, W. H. *J. Phys. Chem. Lett.* **2010**, *1*, 891−894.

(21) Kelly, A.; Rhee, Y. M. *J. Phys. Chem. Lett.* **2011**, *2*, 808−812.

(22) Chen, X.; Silbey, R. J. *J. Phys. Chem. B* **2011**, *115*, 5499−5509.

(23) Renaud, N.; Ratner, M. A.; Mujica, V. *J. Chem. Phys.* **2011**, *135*, 075102.

(24) Olbrich, C.; Jansen, T. L. C.; Liebers, J.; Aghtar, M.; Strümpfer, J.; Schulten, K.; Knoester, J.; Kleinekathöfer, U. *J. Phys. Chem. B* **2011**, *115*, 8609−8621.

(25) Shim, S.; Rebentrost, P.; Valleau, S.; Aspuru-Guzik, A. *Biophys. J.* **2012**, *102*, 649−660.

(26) Ishizaki, A.; Fleming, G. R. *J. Phys. Chem. B* **2011**, *115*, 6227−6233.

(27) MacKerell, A. D., Jr.; et al. *J. Phys. Chem. B* **1998**, *102*, 3586−3616.

(28) MacKerell, A. D., Jr.; Feig, M.; Brooks, C. L., III *J. Comput. Chem.* **2004**, *25*, 1400−1415.

(29) Cornell, W. D.; Cieplak, P.; Bayly, C. I.; Gould, I. R.; Merz, K. M., Jr.; Ferguson, D. M.; Spellmeyer, D. C.; Fox, T.; Caldwell, J. W.; Kollman, P. A. *J. Am. Chem. Soc.* **1995**, *117*, 5179−5197.

(30) Ishizaki, A.; Fleming, G. R. *J. Chem. Phys.* **2009**, *130*, 234110.

(31) Ishizaki, A.; Fleming, G. R. *J. Chem. Phys.* **2009**, *130*, 234111.

(32) Jang, S.; Cheng, Y.-C.; Reichman, D. R.; Eaves, J. D. *J. Chem. Phys.* **2008**, *129*, 101104.

(33) Kim, H.; Nassimi, A.; Kapral, R. *J. Chem. Phys.* **2008**, *129*, 084102.

(34) Nassimi, A.; Bonella, S.; Kapral, R. *J. Chem. Phys.* **2010**, *133*, 134115.

(35) Madjet, M. E.; Abdurahman, A.; Renger, T. *J. Phys. Chem. B* **2006**, *110*, 17268−17281.

(36) Krueger, B. P.; Scholes, G. D.; Fleming, G. R. *J. Phys. Chem. B* **1998**, *102*, 5378−5386.

(37) Olbrich, C.; Kleinekathöfer, U. *J. Phys. Chem. B* **2010**, *114*, 12427−12437.

(38) Bayly, C. I.; Cieplak, P.; Cornell, W. D.; Kollman, P. A. *J. Phys. Chem.* **1993**, *97*, 10269−10280.

(39) Wang, J.; Cieplak, P.; Kollman, P. A. *J. Comput. Chem.* **2000**, *21*, 1049−1074.

(40) Adolphs, J.; Müh, F.; Madjet, M. E.-A.; Renger, T. *Photosynth. Res.* **2008**, *95*, 197−209.

(41) Renger, T. *Photosynth. Res.* **2009**, *102*, 471−485.

(42) Park, J. W.; Kim, H. W.; Song, C.-I.; Rhee, Y. M. *J. Chem. Phys.* **2011**, *135*, 014107.

(43) Maroncelli, M.; Fleming, G. R. *J. Chem. Phys.* **1988**, *89*, 5044−5069.

(44) Kumar, P. V.; Maroncelli, M. *J. Chem. Phys.* **1995**, *103*, 3038−3060.

(45) Ingrosso, F.; Ladanyi, B. M.; Mennucci, B.; Elola, M. D.; Tomasi, J. *J. Phys. Chem. B* **2005**, *109*, 3553−3564.

(46) Martins, L. R.; Skaf, M. S. *Chem. Phys. Lett.* **2003**, *370*, 683−689.

(47) Rasmussen, T. D.; Ren, P.; Ponder, J. W.; Jensen, F. *Int. J. Quantum Chem.* **2007**, *107*, 1390−1395.

(48) Olbrich, C.; Strümpfer, J.; Schulten, K.; Kleinekathöfer, U. *J. Phys. Chem. Lett.* **2011**, *2*, 1771−1776.

(49) Furse, K. E.; Lindquist, B. A.; Corcelli, S. A. *J. Phys. Chem. B* **2008**, *112*, 3231−3239.

(50) Furse, K. E.; Corcelli, S. A. *J. Am. Chem. Soc.* **2008**, *130*, 13103−13109.

(51) Furse, K. E.; Corcelli, S. A. *J. Am. Chem. Soc.* **2011**, *133*, 720−723.

(52) Song, C.-I.; Rhee, Y. M. *J. Am. Chem. Soc.* **2011**, *133*, 12040−12049.

(53) Freiberg, A.; Lin, S.; Timpmann, K.; Blankenship, R. E. *J. Phys. Chem. B* **1997**, *101*, 7211−7220.
(54) Our models are built for the single excitation subspace and have the gap energy between the ground-state subspace and the single excitation subspace as undetermined. Thus, a constant shift needs to be added for obtaining absorption spectra. We have set this shift so that the peak centers overlap with each other.
(55) McCutcheon, D. P. S.; Nazir, A. *J. Chem. Phys.* **2011**, *135*, 114501.
(56) Turner, D. B.; Wilk, K. E.; Curmi, P. M. G.; Scholes, G. D. *J. Phys. Chem. Lett.* **2011**, *2*, 1904−1911.
(57) Sarovar, M.; Ishizaki, A.; Fleming, G. R.; Whaley, K. B. *Nature Phys.* **2010**, *6*, 462−467.
(58) Hill, S.; Wootters, W. K. *Phys. Rev. Lett.* **1997**, *78*, 5022−5025.
(59) Brumer, P.; Shapiro, M., ArXiv:1109.0026.
(60) Pelzer, K. M.; Griffin, G. B.; Gray, S. K.; Engel, G. S. *J. Chem. Phys.* **2012**, *136*, 164508.
(61) Fleming, G. R.; Cho, M. *Annu. Rev. Phys. Chem.* **1996**, *47*, 109−134.
(62) Xu, Q.-H.; Scholes, G. D.; Yang, M.; Fleming, G. R. *J. Phys. Chem. A* **1999**, *103*, 10348−10358.
(63) Vlaming, S. M.; Silbey, R. J. *J. Chem. Phys.* **2012**, *136*, 055102.
(64) Olbrich, C.; Strümpfer, J.; Schulten, K.; Kleinekathöfer, U. *J. Phys. Chem. B* **2011**, *115*, 758−764.
(65) Müh, F.; Madjet, M. E.-A.; Adolphs, J.; Abdurahman, A.; Rabenstein, B.; Ishikita, H.; Knapp, E.-W.; Renger, T. *Proc. Natl. Acad. Sci. U.S.A.* **2007**, *104*, 16862−16867.
(66) Panitchayangkoon, G.; Voronine, D. V.; Abramavicius, D.; Caram, J. R.; Lewis, N. H. C.; Mukamel, S.; Engel, G. S. *Proc. Natl. Acad. Sci. U.S.A.* **2011**, *108*, 20908−20912.
(67) Brixner, T.; Stenger, J.; Vaswani, H. M.; Cho, M.; Blankenship, R. E.; Fleming, G. R. *Nature* **2005**, *434*, 625−628.
(68) We note that there are recent reports about the EET process starting from the missing BChl-8, where the energy transfer is demonstrated to become remarkably different with suppression in the pathway involving BChl-6. See, for example: Moix, J.; Wu, J.; Huo, P.; Coker, D.; Cao, J. *J. Phys. Chem. Lett.* **2011**, *2*, 3045−3052. Investigating this aspect with all-atom non-adiabatic simulations will involve an additional and more demanding FMO trimer system, and we would rather leave this issue as an open question in this work.
(69) Hildner, R.; Brinks, D.; van Hulst, N. F. *Nature Phys.* **2011**, *7*, 172−177.
(70) Alicki, R.; Miklaszewski, W. *J. Chem. Phys.* **2012**, *136*, 134103.
(71) Caycedo-Soler, F.; Chin, A. W.; Almeida, J.; Huelga, S. F.; Plenio, M. B. *J. Chem. Phys.* **2012**, *136*, 155102.
(72) Kapral, R.; Ciccotti, G. *J. Chem. Phys.* **1999**, *110*, 8919−8929.
(73) van der Spoel, D.; Lindahl, E.; Hess, B.; Groenhof, G.; Mark, A. E.; Berendsen, H. J. C. *J. Comput. Chem.* **2005**, *26*, 1701−1718.
(74) Ben-Shem, A.; Frolow, F.; Nelson, N. *FEBS Lett.* **2004**, *564*, 274−280.
(75) Foloppe, N.; Ferrand, M.; Breton, J.; Smith, J. C. *Proteins* **1995**, *22*, 226−244.
(76) Hess, B.; Bekker, H.; Berendsen, H. J. C.; Fraaije, J. G. E. M. *J. Comput. Chem.* **1997**, *18*, 1463−1472.
(77) Berendsen, H. J. C.; Postma, J. P. M.; van Gunsteren, W. F.; DiNola, A.; Haak, J. R. *J. Chem. Phys.* **1984**, *81*, 3684−3690.
(78) Darden, T.; York, D.; Pedersen, L. *J. Chem. Phys.* **1993**, *98*, 10089−10092.
(79) Becke, A. D. *Phys. Rev. A* **1988**, *38*, 3098−3100.
(80) Lee, C.; Yang, W.; Parr, R. G. *Phys. Rev. B* **1988**, *37*, 785−789.
(81) Shao, Y.; et al. *Phys. Chem. Chem. Phys.* **2006**, *8*, 3172−3191.